JNK-dependent intestinal barrier failure disrupts host–microbe homeostasis during tumorigenesis

Jun Zhou[a] and Michael Boutros[a,1]

[a]Division Signaling and Functional Genomics, Department for Cell and Molecular Biology, Medical Faculty Mannheim, German Cancer Research Center and Heidelberg University, D-69120 Heidelberg, Germany

Edited by Barry J. Thompson, The Francis Crick Institute, London, United Kingdom, and accepted by Editorial Board Member Tak W. Mak March 7, 2020 (received for review August 12, 2019)

In all animals, the intestinal epithelium forms a tight barrier to the environment. The epithelium regulates the absorption of nutrients, mounts immune responses, and prevents systemic infections. Here, we investigate the consequences of tumorigenesis on the microbiome using a *Drosophila* intestinal tumor model. We show that upon loss of BMP signaling, tumors lead to aberrant activation of JNK/Mmp2 signaling, followed by intestinal barrier dysfunction and commensal imbalance. In turn, the dysbiotic microbiome triggers a regenerative response and stimulates tumor growth. We find that inhibiting JNK signaling or depletion of the microbiome restores barrier function of the intestinal epithelium, leading to a reestablishment of host–microbe homeostasis, and organismic lifespan extension. Our experiments identify a JNK-dependent feedback amplification loop between intestinal tumors and the microbiome. They also highlight the importance of controlling the activity level of JNK signaling to maintain epithelial barrier function and host–microbe homeostasis.

stem cells | epithelial barrier defects | host–microbe homeostasis | JNK | *Drosophila*

The intestinal epithelium forms a physical barrier that allows selective absorption of nutrients, prevents invasion by pathogens, and mounts immune responses. In *Drosophila*, the intestinal epithelium contains highly proliferative intestinal stem cells (ISCs) that produce progenitor cells called enteroblast (EBs). EBs differentiate into either enterocytes (ECs) or enteroendocrine cells to ensure homeostatic turnover of the tissue (1). Several well-conserved signaling pathways, including Notch, BMP, Wnt, JAK/STAT, and Ras, are required for maintaining intestinal homeostasis and their dysregulation can lead to tumor formation in the *Drosophila* intestine (2–9). Across the animal kingdom, the intestinal epithelium is exposed to a dynamic and metabolically complex bacterial community. Host–microbiome interactions play important roles in maintaining organismal homeostasis, influence the development of the host immune system, and help to digest and absorb nutrients (10–12). While it has become evident that the microbiome is important for organismal health, how changes in host–microbiome interactions contribute to tumorigenesis remains controversial (13).

Due to the low diversity of its intestinal microbiota and powerful genetic tools, *Drosophila* has become an important model system to study host–microbe interactions. In *Drosophila*, the microbiota has been reported to be involved in host development (14–19), influencing lifespan (20–23) and affecting animal behavior and disease (24–28).

In this study, we created an inducible tumor model by tissue-specific depletion of BMP signaling pathway components and investigated its effect on host–microbe interactions. We show that intestinal tumors lead to epithelial barrier dysfunction, which in turn promotes commensal dysbiosis with an increase in microbial load and a decrease in microbial diversity. Dysbiosis further stimulates intestinal regeneration and tumor growth. Mechanistically, we provide evidence that tumor-related JNK hyperactivation leads to barrier loss, dysbiosis, and increased mortality. In contrast, either JNK inhibition or microbiota depletion reverses these phenotypes. Thus, our findings support a model whereby the gut microbiome is neither a driver nor passenger but acts as part of a self-enforcing feedback loop that promotes further intestinal barrier dysfunction and tumorigenesis through the activation of JNK/Mmp2 signaling.

Results

The Intestinal Microbiome Promotes BMP Loss-Induced Tumorigenesis. Dpp/BMP signaling in *Drosophila* is activated by dimers of Dpp ligands that bind to type I (Thickveins; Tkv) and type II (Punt) receptors. Activated Tkv, in turn, phosphorylates the *Drosophila* Smad Mother-against-Dpp (Mad), which interacts with the co-Smad Medea (Med) and Schnurri (Shn). Inactivation of BMP pathway components in the *Drosophila* midgut leads to intestinal tumor phenotypes similar to juvenile polyposis syndrome, a congenital condition with an increased risk of developing gastrointestinal cancer (2). Previous studies reported multiple roles of Dpp/BMP signaling in intestinal homeostasis in *Drosophila*, including ISC self-renewal, EB to EC differentiation, copper cell differentiation, and EC survival (2, 22, 29–32).

Using the inducible escargot-Flip Out (esgts F/O) system to generate GFP-marked mosaic clones (33), we induced the expression of hairpin RNA interference (RNAi) constructs targeting BMP-signaling components in ISCs, EBs (escargot$^+$ [esg$^+$] cells), and all their progeny. In these clones, RNAi-expressing cells and their progeny are marked with GFP, while already existing differentiated cells do not express the RNAi construct and remain GFP$^-$ (Fig. 1*A*). Upon *Med* or *Shn* RNAi, we found disorganized, multilayered epithelial clones as compared to a single epithelial layer in controls (Fig. 1 *B–D*). The effect of the RNAi was

Significance

The intestinal epithelium forms a tight barrier to the environment and is constantly regenerated. Precise control of barrier function and tissue renewal is important to maintain homeostasis. Using an inducible tumor model in the *Drosophila* intestine, this study shows that tumor progression disrupts the intestinal barrier and leads to commensal dysbiosis, thereby further fueling tumor growth. This reenforcing feedback loop can be interrupted by treatments with JNK inhibitor or antibiotics.

Author contributions: J.Z. and M.B. designed research; J.Z. performed research; J.Z. and M.B. analyzed data; and J.Z. and M.B. wrote the paper.

The authors declare no competing interest.

This article is a PNAS Direct Submission. B.J.T. is a guest editor invited by the Editorial Board.

[1]To whom correspondence may be addressed. Email: m.boutros@dkfz.de.

This article contains supporting information online at https://www.pnas.org/lookup/suppl/doi:10.1073/pnas.1913976117/-/DCSupplemental.

First published April 10, 2020.

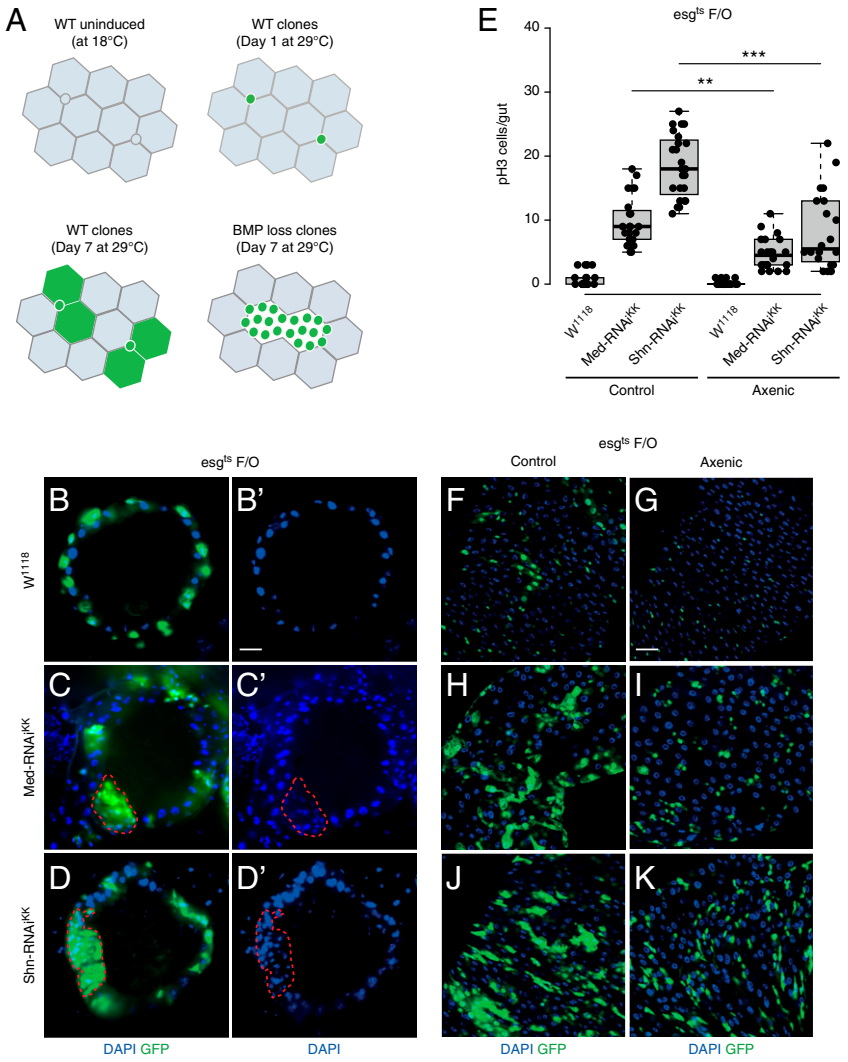

Fig. 1. The intestinal microbiome promotes tumorigenesis. (*A*) The diagram displays the *esg^{ts}F/O* system. (*Upper Left*) the *F/O* system is inactivated by the temperature-sensitive repressor Gal80^{ts} at 18 °C. (*Upper Right*) At day 1, Gal80^{ts} is suppressed at 29 °C and esg-Gal4 will drive the expression of UAS-GFP and UAS-flippase, in turn, activating the Act > CD2 > Gal4 cassette. (*Lower Left*) At day 7, the F/O system will express UAS-GFP and transgene of interest in the progenitor cells from stem cells and enteroblast due to the ubiquitous Act-Gal4 expression. (*Lower Right*) At day 7, the F/O system-activated Mad, Med, or Shn RNAi transgene and GFP causes accumulation of small nuclei GFP^{+} cells. (*B–D*) Representative images of cross-sections of *esg^{ts} F/O > W^{1118}* (*B*), *Med-RNAi^{KK}* (*C*), and *Shn-RNAi^{KK}* (*D*) midgut after 10 d at 29 °C. GFP (green): *Act-GFP*; DAPI (blue): DNA. F/O clones are indicated by a dashed red line. (Scale bar, 30 μm.) (*E*) Quantification of pH3^{+} cells per adult midgut of the indicated genotypes in standard and antibiotics-treated fly food after 5 d at 29 °C. The axenic flies were dissected after 5-d RNAi induction to avoid contamination. Significance values are indicated by asterisks: $^{**}P < 0.01$; $^{***}P < 0.001$. (*F–K*) Representative images of the posterior midgut of *esg^{ts}F/O > W^{1118}* (*F* and *G*), *esg^{ts} F/O > Med-RNAi^{KK}* (*H* and *I*), and *esg^{ts} F/O > Shn-RNAi^{KK}* (*J* and *K*) flies raised in axenic condition, stained with pH3 antibody in red. *Act-GFP* is shown in GFP, nuclei are stained with DAPI (blue). (Scale bar, 30 μm.)

confirmed using the wing-specific driver Nubbin-Gal4, which mediated the expected BMP loss-of-function phenotypes (*SI Appendix*, Fig. S1 *A–D*) (32). In addition, ISC proliferation phenotypes were confirmed by multiple independent RNAi lines (*SI Appendix*, Fig. S1*E*) and were also observed after tissue-specific CRISPR knockout of *Mad* or *Med* (*SI Appendix*, Fig. S1*Q*). Together, these results show that inactivation of BMP signaling causes accumulation of stem cells and a multilayered epithelium, resembling previously described intestinal tumors induced by dysregulation of *Notch* and *Sox21a* (3, 6).

Next, to gain insights into the contribution of the microbiota to intestinal tumor growth, we depleted the intestinal microbiome by raising flies under axenic condition or feeding antibiotics. We observed that *Med* or *Shn* RNAi animals raised under germ-free conditions developed fewer *esg*$^{+}$ cell clusters and showed a significant decrease in stem cell mitosis (Fig. 1 *E–K*). In addition, microbiota depletion reduces tumor-related increase in stem cell proliferation in *Shn* RNAi flies (*SI Appendix*, Fig. S1 *F–L*). Consistently, knockouts of *Med* and *Mad* by tissue-specific CRISPR/Cas9 also showed a significant reduction in tumor growth upon antibiotic feeding as compared to control conditions (*SI Appendix*, Fig. S1 *M–Q*). We confirmed that antibiotic treatment significantly reduced the gut microbiome in control and *Shn* RNAi flies (*SI Appendix*, Fig. S1*R*). Taken together, these data indicate that the depletion of the microbiome impacts stem cell proliferation and inhibits tumor growth.

Intestinal Tumors Influence the Microbiota. To assess whether the induction of intestinal tumors alters the microbiome, we first monitored changes in gut bacterial load. Interestingly, we found a significant increase in bacterial load upon *Mad*, *Med*, and *Shn* RNAi, as well as after tissue-specific *Med* knockout (Fig. 2 *A* and *B*).

In addition, we confirmed an age-dependent increase in microbial load in the *Shn* RNAi intestine (*SI Appendix*, Fig. S2*A*). Similarly, *Shn*-RNAi flies displayed an increased intestinal stem cell proliferation during aging (*SI Appendix*, Fig. S2*B*).

To further investigate changes in the microbial composition, we conducted 16S rDNA sequencing on Shn RNAi and control intestines. The experiments revealed an enrichment of *Acetobacteria* species concurrent with a significant reduction in overall microbial diversity in the intestine of tumor-bearing flies (Fig. 2*C*). Since the comparative analysis did not provide information about the extent of changes in taxa abundance and changes in the overall microbiome (34), we examined the load of various bacteria by colony formation unit (CFU) assays on selective mediums for *Acetobacteriaceae* and other bacteria (NR) (20, 35), as well as by taxa-specific 16S qPCR (36, 37). In these experiments, we observed intestinal dysbiosis in Dpp/BMP knockdown conditions (both *Mad* and *Med* RNAi, referred to as *Mad/Med-RNAi*, *Shn* RNAi), as shown in *SI Appendix*, Fig. S2 *C* and *D*. A similar dysbiosis was observed in *Notch*-depleted (*N* RNAi) animals as an independent means to induce stem cell tumors (*SI Appendix*, Fig. S2*D*). Furthermore, animals with intestinal-specific *Med* knockouts showed a significant increase in *Acetobacteria* and other bacteria upon growth on nutrient-rich medium (*SI Appendix*, Fig. S2*E*). Together, these data demonstrate an overall increased bacterial load and a lower microbial diversity in the intestines of tumor-bearing flies.

Previous work showed that BMP signaling determines copper cell differentiation and its inactivation leads to decline of the acidic stomach-like copper cell region (CCR) in the middle midgut (2, 20, 22, 29–32). In addition, age-related CCR decline disrupts the distribution and diversity of gut commensals (22). To exclude that tumor-related microbial dysbiosis is caused by decline of the acidic stomach-like CCR, we assessed the function of the CCR by feeding control and tumor-bearing flies with a diet containing a pH indicator. These experiments indicated that the tumor flies display dysbiotic phenotype at early time points (day 5 and day 8), but maintain the acidity in the CCR (*SI Appendix*, Fig. S2 *A*, *F*, and *G*). In addition, the expression of CCR-specific vacuolar-type H^+ ATPase, *Vha100-4*, remained at a similar level in the tumor intestine compared to the control tissue (*SI Appendix*, Fig. S2*H*). These results suggest that the tumor-induced dysbiosis is not caused by BMP-related decline in CCR function.

Intestinal Tumorigenesis Impairs Epithelial Barrier Functions. Complex rearrangements of cell–cell adhesion are required for shaping the intestine and for maintaining tissue integrity during development (38, 39). The maintenance of the intestinal barrier is essential for preserving homeostasis and organismal health (36, 37). To test whether loss of BMP-induced intestinal tumors disrupts barrier function by altering cell adhesion molecules, we monitored the expression of septate junction proteins Disk large (Dlg) and Fascillin III (FasIII) using immunostaining. We observed significant changes in the septate junction proteins (Dlg, FasIII), which were either mislocalized or reduced (Fig. 3 *A*–*F* and *SI Appendix*, Fig. S3 *A* and *B*). These results show that the septate junctions between tumor and intestinal cells are disrupted in the tissue.

To further explore whether tumor-bearing flies show barrier defects, we fed flies with a blue dye to monitor intestinal epithelial integrity. Feeding this dye to flies with barrier defects often leads to dye leakage into the body cavity [also referred to as "smurf" assay (40)]. Flies with tumors frequently showed impaired intestinal barriers, with a significantly higher fraction of nonabsorbable blue dye leakage in the fly compared to controls (Fig. 3 *G* and *H*). These results suggest that tumor growth induces epithelial barrier defects. We also observed that Med- and Shn-depleted midguts were shorter when compared to control midguts (*SI Appendix*, Fig. S3 *C*–*E* and *H*). Similarly, *Med* CRISPR knockouts also showed a shorter gut phenotype (*SI Appendix*, Fig. S3 *F*, *G*, and *I*).

Clark et al. (36) reported that intestinal barrier loss leads to immune activation and increased tissue regeneration. To further test whether tumor growth impairs barrier function, we examined in more detail the expression of genes involved in immune activation (*Peptidoglycan Recognition Protein SC2*, *PGRP-SC2*; *Diptericin*, *Dpt*), reactive oxygen species (ROS) production (*Duox*), cytokine for STAT signaling activation (Upd3), and stress signaling (*Kayak* [*Kay*], the homolog of *Fos*; *Puckered* [*Puc*]) in the intestines of *Shn* RNAi flies. qRT-PCR from dissected intestine revealed that the JNK signaling pathway components *Kay* and *Puc* were highly induced in *Mad*/*Med*-RNAi or *Shn*-RNAi flies, as well as the cytokine Upd3 (*SI Appendix*, Fig. S3 *J* and *K*). We also observed a decrease in *PGRP-SC2* expression and an increase in *Dpt* levels, indicative of immune activation in *Mad*/*Med*-RNAi or *Shn*-RNAi intestines (*SI Appendix*, Fig. S3 *J* and *K*). *PGRP-SC2* is a known negative regulator of the Relish pathway and its suppression has been linked

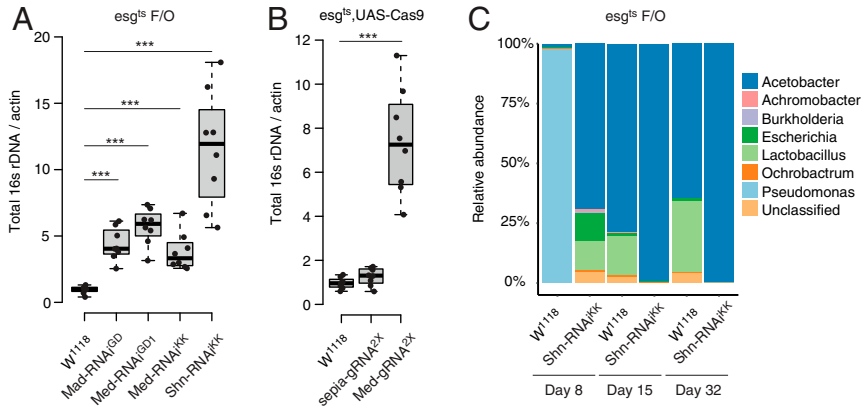

Fig. 2. Intestinal tumors induce changes in the microbiome. (*A*) Bacterial levels in the intestines of esg^{ts} *F/O* > *Mad-RNAi*^{GD}, esg^{ts} *F/O* > *Med-RNAi*$^{GD-1}$, esg^{ts} *F/O* > *Med-RNAi*^{KK}, esg^{ts} *F/O* > *Shn-RNAi*^{KK}, and esg^{ts} *F/O* > W^{1118}, assayed by qPCR of 16S rDNA gene at 15 d at 29 °C. The flies were killed after 15-d RNAi induction to ensure more robust dysbiotic phenotype, as shown in *SI Appendix*, Fig. S2*A*. (*B*) Bacterial levels in the intestines of esg^{ts}; *UAS-Cas9* > *Med-gRNA*^{2X}, esg^{ts}; *UAS-Cas9* > *sepia-gRNA*^{2X} and esg^{ts}; *UAS-Cas9* > W^{1118}, assayed by qPCR of 16S rDNA gene at 18 °C for 30 d after inducing mutagenesis. *sepia-gRNA*^{2X} was used as a negative control. (*C*) The commensal composition of esg^{ts} *F/O* > *Shn-RNAi*^{KK} and esg^{ts}*F/O* > W^{1118} midguts after 8, 15, and 32 d at 29 °C. Bar charts show the top eight bacterial genera determined by 16S rDNA sequencing. Significance values are indicated by asterisks: ***$P < 0.001$.

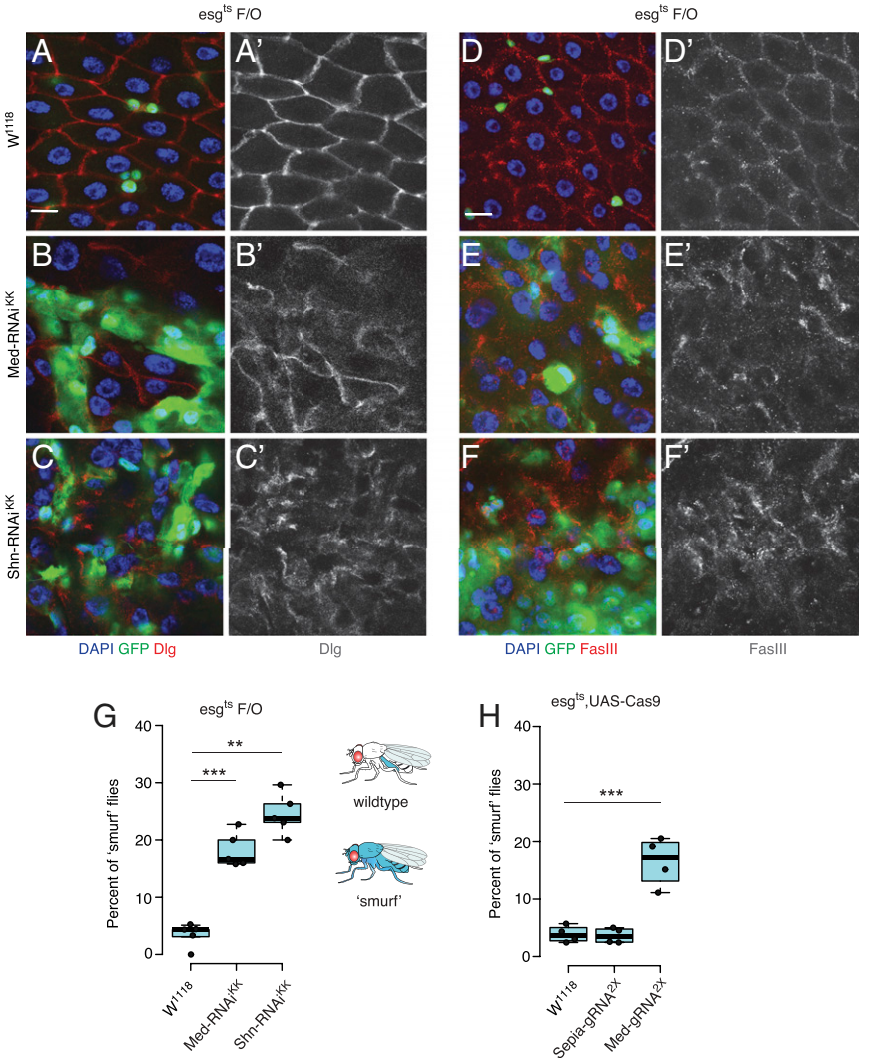

Fig. 3. Tumor growth leads to disruption of epithelial barrier function. (*A–C*) Representative images of the posterior midgut of *esg^ts F/O > W^1118* (*A*), *esg^ts F/O > Med-RNAi^KK* (*B*), and *esg^ts F/O > Shn-RNAi^KK* (*C*) flies at 29 °C for 7 d, stained with anti-Dlg antibodies. (*D–F*) Representative images of the posterior midgut of *esg^ts F/O > W^1118* (*D*), *esg^ts F/O > Med-RNAi^KK* (*E*), and *esg^ts F/O > Shn-RNAi^KK* (*F*) flies at 29 °C for 7 d, stained with anti-FasIII antibodies. (Scale bars, 10 μm.) (*G* and *H*) Smurf assay for gut integrity and barrier defects of indicated genotype. A high percentage of smurf flies are shown in the group of *Med-RNAi^KK*, *Shn-RNAi^KK* (*G*) or *Med-gRNA^2X* (*H*) flies compared to the controls (*W^1118* or *sepia-gRNA^2X*). The smurf assay on RNAi or CRISPR experiment is monitored at 29 °C for 25 d or at 18 °C for 45 d after inducing mutagenesis. Significance values are indicated by asterisks: $^{**}P < 0.01$; $^{***}P < 0.001$.

to commensal dysbiosis (20). We further found that the NADPH oxidase (*Duox*), responsible for producing microbial ROS in response to infection (41), showed a significantly decreased expression in the tumor intestine (*SI Appendix*, Fig. S3*K*). Together, these results indicate that intestinal tumors lead to activation of stress and immune signaling, shorter gut length, and impairs intestinal barrier function.

JNK Activation Contributes to Tumor Growth. To understand the mechanisms promoting tumor growth and dysbiosis, we next assessed JNK signaling activity in *Med-* or *Shn*-depleted midguts. JNK was activated in the intestine after *Med* or *Shn* depletion, as measured by *Kay* and *puc* up-regulation (*SI Appendix*, Fig. S3 *J* and *K*). Further experiments using a *puckered-lacZ* (*puc-lacZ*) reporter showed that JNK signaling was activated not only within the tumor but also in the nearby ECs (Fig. 4 *A–C*). Moreover, CRISPR/Cas9-mediated *Mad* or *Med* intestinal knockouts showed a similar up-regulation of *puc-lacZ* signal (Fig. 4 *E–G*). Consistently, we observed an increase of phospho-JNK levels in tumor intestine (*SI Appendix*, Fig. S4 *A–C*).

We next asked whether JNK signaling is required for BMP-dependent tumor growth. To this end, we either inhibited or activated JNK signaling by expressing a dominant-negative form of *Basket* (*Bsk^DN*), by *Kay* RNAi, or by the introduction of a heterozygous mutation of *Puckered* (*Puc^E69*/+), a negative JNK pathway regulators (42). We found that activating JNK signaling by removing one copy of *Puckered* significantly induced ISC division and tumor load in the *Shn*-depleted intestine (Fig. 4*D* and *SI Appendix*, Fig. S4 *D–H*). Conversely, JNK suppression (*Bsk^DN* or *Kay-RNAi*) largely reduced ISC proliferation and tumor burden (Fig. 4*D* and *SI Appendix*, Fig. S4 *D–H*). In addition, JNK activation induced *Mad* or *Med* knockout-related tumor phenotype with elevated stem cell mitosis (Fig. 4*H*). These results suggest that activation of JNK contributes to intestinal tumorigenesis.

JNK/Mmp2 Signaling Contributes to Intestinal Barrier Loss and Dysbiosis. To test whether tumor-related JNK activation induces intestinal barrier dysfunction, we monitored the septate junction proteins and tissue integrity in the tumor-bearing flies

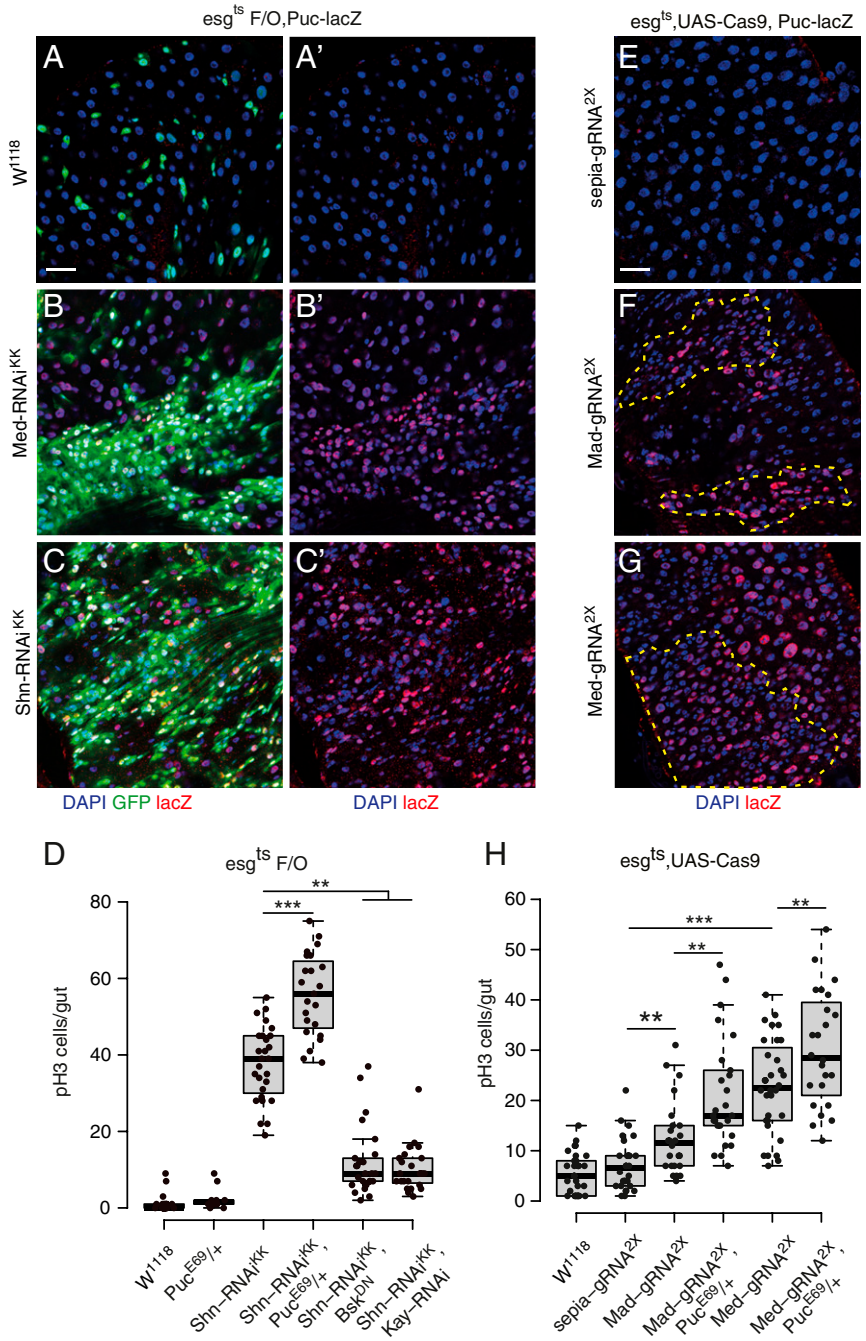

Fig. 4. BMP-loss induced tumors activate JNK. (*A*–*C*) The *puc-lacZ* expression in the midgut of *esg^{ts}F/O* > *W^{1118}* (*A*), *esg^{ts} F/O* > *Med-RNAi^{KK}* (*B*), and *esg^{ts} F/O* > *Shn-RNAi^{KK}* (*C*) with anti–β-Galactosidase staining at 29 °C for 7 d. (Scale bar, 30 μm.) (*D*) Quantification of pH3^{+} cells per adult midgut of the indicated genotypes at 29 °C for 7 d. (*E*–*G*) Immunofluorescence images of midguts of *esg^{ts};UAS-Cas9* > *Mad-gRNA^{2X}* (*F*) or *Med-gRNA^{2X}* (*G*) or *sepia-gRNA^{2X}* (*E*) with anti–β-Galactosidase staining at 18 °C for 30 d after inducing mutagenesis. The "tumor"-like small nuclei cell clusters in the mutant intestine are indicated by yellow dashed line. (Scale bar, 30 μm.) (*H*) Quantification of pH3^{+} cells per adult midgut of the indicated genotypes at 18 °C for 30 d. Significance values are indicated by asterisks: $^{**}P < 0.01$; $^{***}P < 0.001$.)

after modulation of JNK signaling. We found that JNK activation (*Puc^{E69}*/+) enhanced the mislocalization and loss of septate junction proteins (Dlg, FasIII) in *esg^{ts}F/O*-driven *Shn* RNAi flies (Fig. 5 *A*–*C* and *SI Appendix*, Fig. S4 *I*–*K*). In contrast, JNK suppression partially rescued the loss of septate junction protein phenotype in the tumor intestine (Fig. 5*D*). *Shn* RNAi flies with JNK activation displayed an even shorter midgut and this phenotype was completely suppressed by JNK inhibition (*Bsk^{DN}* or *Kay*-RNAi) (*SI Appendix*, Fig. S4 *D*–*H* and *L*). JNK suppression (*Bsk^{DN}* or *Kay-RNAi*) also extended the lifespan of flies with tumor (*SI Appendix*, Fig. S4 *M* and *N*), while JNK activation enhanced the mortality of tumor-bearing flies (*SI Appendix*, Fig. S4 *M* and *N*).

To explore how JNK activation contributes to increased mortality in tumor-bearing flies, we fed flies with blue dye to monitor intestinal epithelial integrity. In tumor-bearing flies, we observed a significant breakdown of tissue integrity and decreasing JNK activity resulting in a reduced proportion of smurf

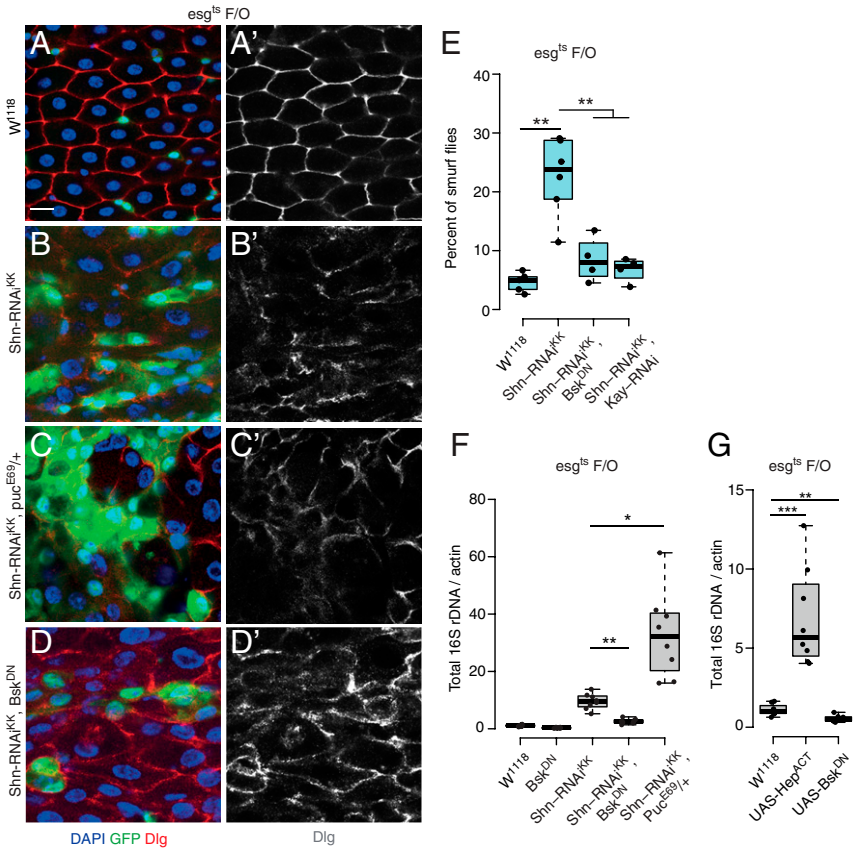

Fig. 5. Tumor-induced JNK activation disrupts epithelial function and causes dysbiosis. (*A–D*) Representative images of the posterior midgut of *esg*^{ts} *F/O* > *w1118*(*A*), *esg*^{ts}*F/O* > *Shn-RNAi* (*B*), *esg*^{ts} *F/O* > *Shn- RNAi*^{KK}; *Puc*^{E69}/+ (*C*), and *esg*^{ts} *F/O* > *Shn-RNAi*^{KK}; *UAS-Bsk*^{DN} (*D*) flies stained with Dlg antibody. (Scale bar, 10 μm.) (*E*) Smurf assay for gut integrity and barrier defects of indicated genotype at 29 °C for 25 d. (*F*) The bacterial level in the intestine of *esg*^{ts} *F/O* > *UAS-Bsk*^{DN}, *esg*^{ts}*F/O* > *Shn-RNAi*^{KK}, *esg*^{ts} *F/O* > *Shn-RNAi*^{KK};*UAS-Bsk*^{DN}, *esg*^{ts} *F/O* > *Shn- RNAi*^{KK}, *Kay-RNAi* and *esg*^{ts} *F/O* > *W*^{1118} flies, assayed by qPCR of 16S rDNA gene at 29 °C for 15 d. (*G*) The bacterial level in the intestine of *esg*^{ts} *F/O* > *UAS-Hep*^{ACT}, *esg*^{ts} *F/O* > *UAS-Bsk*^{DN} flies, assayed by qPCR of 16S rDNA at 29 °C for 12 d. Significant differences are indicated with asterisks: *$P < 0.05$; **$P < 0.01$; ***$P < 0.001$.

and dysbiotic phenotypes (Fig. 5*E* and *SI Appendix*, Fig. S4*O*). In addition, we found that JNK activation alone can lead to a loss of Dlg protein in septate junctions and increases intestinal barrier dysfunction (*SI Appendix*, Fig. S5 *A–C*). In Sox21a tumors, JNK-mediated Mmp2 expression can contribute to enterocyte detachment (6). To ask whether Mmps are required for tumor growth, we expressed either *Mmp1* or *Mmp2* using the *esg*^{ts}*F/O* system and monitored the tissue integrity and bacterial load. Ectopic expression of *Mmp2*, but not *Mmp1*, triggered intestinal barrier defect and microbial dysbiosis (*SI Appendix*, Fig. S5 *D* and *E*). Next, we coexpressed *Shn* RNAi and *Mmp2* RNAi using the *esg*^{ts} *F/O* system and monitored stem cell activity (Delta-lacZ or mitotic index), barrier defect, and changes in microbiota. *Mmp2* RNAi effectively reduced *Mmp2* expression in the intestine (*SI Appendix*, Fig. S5*F*). We observed a significant reduction in stem cell proliferation and tumor growth, recovered barrier function, and host–microbe homeostasis upon *Mmp2* depletion (*SI Appendix*, Fig. S5 *G–K*). These results suggest that JNK when is activated it triggers intestinal barrier dysfunction, accelerates tumor growth, and induces dysbiosis through regulating its downstream effector Mmp2.

As the intrinsic JNK activity contributes to BMP-loss–induced tumorigenesis and tissue failure, we hypothesized that JNK is also involved in tumor-related microbiota dysbiosis. We next examined the overall bacterial load in the tumor tissue with aberrant JNK activity by 16S rDNA qRT-PCR. Blocking JNK activity by expressing *Bsk*^{DN} rescued the microbial dysbiosis in the tumor-bearing flies (Fig. 5*F*). In contrast, JNK activation (*Puc*^{E69}/+) enhanced the tumor-related dysbiosis (Fig. 5*F*). Furthermore, *Acetobacter* and *Lactobacilli* increased significantly in tumor-bearing flies. In line with the abovementioned results, JNK suppression largely reduced the microbial dysbiosis as measured by CFUs assays on *Acetobacter*, *Lactobacilli*, and other bacteria populations (*SI Appendix*, Fig. S4*P*). Indeed, the level of intestinal JNK activity is associated with the changes of microbiota (Fig. 5*G*). Hence, these results indicate that high intestinal JNK activity is linked to loss of host–microbe homeostasis.

Intestinal Tumor Regression Restores Epithelial Function and Dysbiotic Phenotype. To explore the temporal link between intestinal tumorigenesis, changes in immune responses, and a dysbiotic microbiome, we designed a time-course experiment using the temperature-controlled *esg*^{ts} *F/O* system. First, we initiated tumor growth by depletion of Med or Shn for 7 d (T7), and subsequently divided the population of flies into two groups that either continuously expressed (T14) or stopped to express the *Shn* or *Med* RNAi transgenes (T7+7) (Fig. 6*A*). We then monitored the expression of genes involved in immune activation (*PGRP-SC1a*, *-b*, *PGRP-SC2*, *Dpt*), stress signaling (*Kay*, *Puc*, *Mmp1*, *Mmp2*), ROS production (*Duox*), internal bacterial load, tumor growth, and tissue morphology.

These experiments showed that the continuous Shn RNAi caused an enhanced tumor growth with more severe tissue morphology defects at T_{14} (Fig. 6*F*) compared to T_7 (Fig. 6*E*),

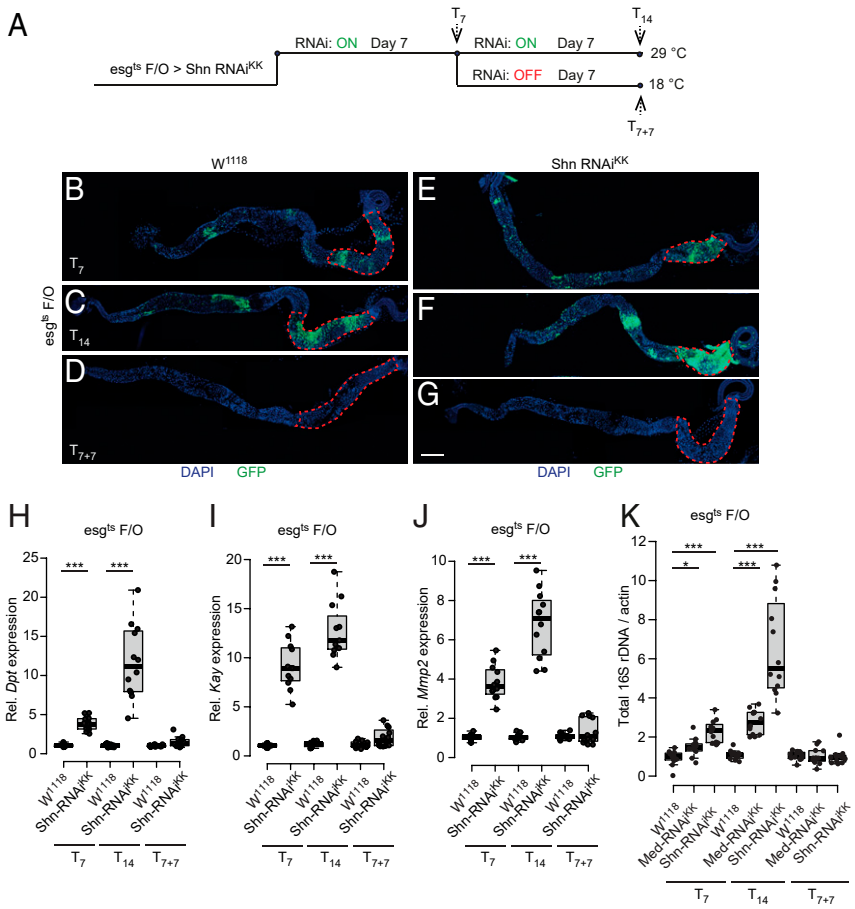

Fig. 6. Regression of intestinal tumor restores epithelial function and reduces the dysbiosis. (*A*) The system to express transgenes in stem cell and its progenitors to initiate intestinal tumor and subsequently remove the tumor in a temperature control manner. (*B–G*) Representative images of midguts of *esg^{ts} F/O > W^{1118}*, *esg^{ts} F/O > Shn-RNAi^{KK}* flies "T_7" (*B* and *E*) or "T_{14}" (*C* and *F*), or "T_{7+7}" (*D* and *G*). Conditions: Tumor start (T7): at 29 °C for 7 d; tumor progression (T14): at 29 °C for 14 d; tumor recovery (T7+7): at 29 °C for 7 d then shifted to 18 °C for another 7 d. *Act-GFP* is shown in GFP, nuclei are stained with DAPI (blue). *B–G* were masked with black shade to cover unrelated tissues for clearer view of target intestine and original images are provided in *SI Appendix*, Fig. S7. (Scale bar, 250 μm.) (*H–J*) qRT-PCR analysis of the intestine shows that the expression levels of Relish (*Dpt*-H) and JNK (*Kay*-I, *Mmp2*-J) pathway component genes are altered in *esg^{ts} F/O > Shn-RNAi^{KK}* flies in the conditions of tumor "start" (T_7), "progression" (T_{14}), and "recovery" groups (T_{7+7}). Significance values are indicated by asterisks: *$P < 0.05$; ***$P < 0.001$. (*K*) Bacterial levels in the intestine of *esg^{ts} F/O > Shn-RNAi^{KK}* and *esg^{ts} F/O > W^{1118}*, assayed by qPCR of 16S rDNA in tumor "start," "progression," and "recovery" conditions.

while no tumor phenotypes were observed in controls at T_7, T_{14}, or T_{7+7} (Fig. 6 *B–D*). This tumor phenotype can be reversed in the T_{7+7} condition by switching off RNAi expression and thereby restoring BMP signaling (Fig. 6*G*). Concurrently, we also observed a reversal of the increased stem cell proliferation and shorter gut phenotype in the T_{7+7} group (*SI Appendix*, Fig. S6 *A* and *B*).

At the molecular level, we found that immune activation in the tumor tissue was restored to the control levels in the tumor T_{7+7} condition, as indicated by the expression of *PGRP-SC1a*, *PGRP-SC1b*, *PGRP-SC2*, and *Dpt* (Fig. 6*H* and *SI Appendix*, Fig. S6 *C–E*). Furthermore, the expression of JNK signaling target genes (*Kay*, *Puc*, *Mmp1*, *Mmp2*) was also reduced to control levels in the T_{7+7} condition (Fig. 6 *I* and *J* and *SI Appendix*, Fig. S6 *F* and *G*). *Duox* expression was also significantly lower in the T_7 and T_{14} groups but returned to normal levels in the T_{7+7} group (*SI Appendix*, Fig. S6*H*). An increase in intestinal bacterial load was observed in the T_7 and T_{14} conditions, whereas the bacterial load in the T_{7+7} conditions returned to a normal level as compared to the control group as well as the ISC proliferation (Fig. 6*K* and *SI Appendix*, Fig. S6*A*). To further confirm the changes of *Alphaproteobacteria* and *Bacillus* bacteria families in the tumor "recovery" group, we used specific primers, as described previously (43), and found that both *Acetobacteraceae* and *Lactobacillus plantarum* levels are increased in the T_7 and T_{14} and returned to a normal level in the T_{7+7} condition (*SI Appendix*, Fig. S6 *I* and *J*). Thus, our data indicate that the altered gut length, increased ISC proliferation, and microbiota dysbiosis are associated with tumor progression and these phenotypes are reversed when tumors disappear.

Removal of Microbiota Restores Intestinal Function in Tumor-Bearing Flies. To determine whether preventing tumor-related dysbiosis can influence intestinal barrier dysfunction and animal health, we treated tumor animals with antibiotics to eliminate bacterial growth at 2 d prior to tumor initiation. The antibiotic treatment caused a significant reduction ($P < 0.05$) in genes involved in stress signaling (*Kay*) and regenerative response (*Upd3*) in the tumor tissue (Fig. 7 *A* and *B*). The expression of the antimicrobial peptide (*Dpt*) was also reduced in the gut of tumor flies upon antibiotics feeding (Fig. 7*C*). In addition, antibiotic-treated tumor animals showed a reduced intestinal barrier failure (Fig. 7*D*). The antibiotic feeding also significantly increased the

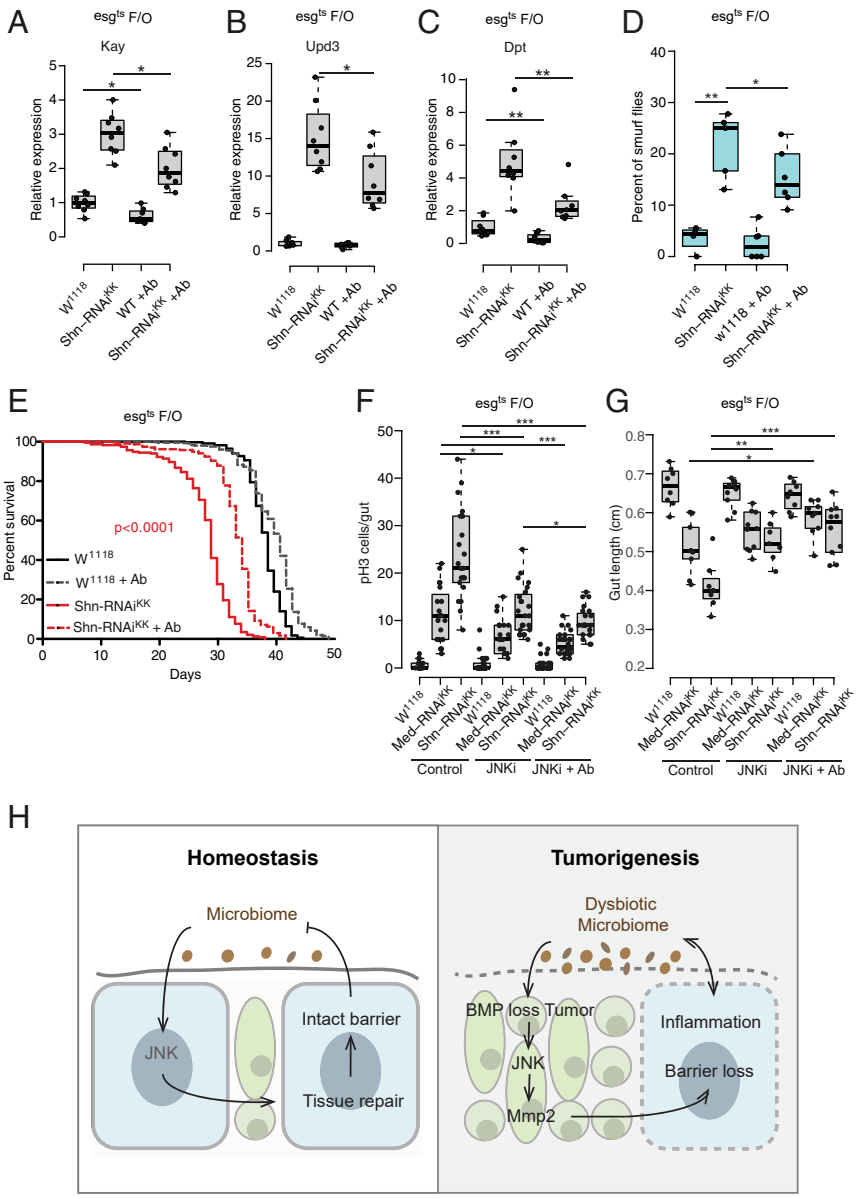

Fig. 7. Depletion of the microbiome or inhibition of JNK signaling restores intestinal function and organismal health. (*A*–*C*) qRT-PCR analysis of the intestine shows that the expression levels of JNK (*Kay*, *A*), regenerative cytokine (Upd3, *B*), and Relish (*Dpt*, *C*) pathway component genes are reduced in *esg*^{ts} *F/O*> *Shn-RNAi*^{KK} flies upon antibiotic feeding at 29 °C for 7 d. (*D*) Smurf assay for gut permeability of indicated genotype at 29 °C for 25 d. Antibiotics feeding reduces Shn-RNAi induced Smurf phenotype. (*E*) The lifespan of Shn-RNAi^{KK} tumor flies compared to control flies on normal or antibiotic food. No antibiotics: *W*^{1118} $n = 341$, *Shn-RNAi*^{KK} $n = 234$; with antibiotics: *W*^{1118} $n = 401$, *Shn-RNAi*^{KK} $n = 239$. (*F*) Quantification of pH3^{+} cells per adult midgut of the indicated genotypes after 8-d RNAi induction in control, JNK inhibitor (SP600125) feeding, and a combination of JNK inhibitor and a mixture of antibiotics. (*G*) Quantification of the length of intestine of *esg*^{ts} *F/O* > *Shn-RNAi*^{KK}, *esgt*^{ts} *F/O* > *Med-RNAi*^{KK}, and *esg*^{ts} *F/O* > *W*^{1118} after 8-d RNAi induction in control, JNK inhibitor (SP600125) feeding and a combination of JNK inhibitor and a mixture of antibiotics. Significance values are indicated by asterisks: $*P < 0.05$; $**P < 0.01$; $***P < 0.001$. (*H*) Model of tumor–microbe interaction. The BMP-defective tumors activate intestinal JNK leading to barrier dysfunction and inflammation, which, in turn, leads to a commensal control loss and further accelerates tumorigenesis.

lifespan of *Shn*-RNAi flies (Fig. 7*E*), indicating tumor-related microbiota is detrimental to barrier-loss–mediated mortality.

To better understand the relationship between intrinsic JNK activation and extrinsic microbiota on intestinal tumor growth, we utilized antibiotic feeding in combination with the JNK inhibitor SP600125. Treatment with a JNK inhibitor alone showed a reduced level of stem cell division and tumor burden and led to a recovery on the gut length of tumor-bearing flies (Fig. 7 *F* and *G*). Interestingly, a combination of antibiotic treatment and JNK inhibitor feeding showed an additive effect on the suppression of stem cell activity and tumor growth (Fig. 7*F*). In addition, the combinatorial treatment showed a better recovery of the gut length phenotype in the tumor flies (Fig. 7*G*). Hence, these results indicate intestinal microbiota and intrinsic JNK activity are both required for tumor growth, whereas a combinatorial targeting shows a beneficial effect on tumor inhibition.

Discussion

Recent studies have investigated tumors that arise by loss of differentiation, accumulation of differentiating stem cells, or stem cell hyperproliferation in adult *Drosophila* intestine (2–9, 44). Loss of BMP signaling through mutation in SMAD4 or

BMPR1A is a known cause of gastrointestinal cancers in human (45). Similarly, inactivation of BMP pathway components also leads to intestinal tumor phenotypes in *Drosophila* (2). In this study, we used an inducible intestinal tumor model by independent RNAi constructs or CRISPR/Cas9 mutagenesis targeting BMP signaling to investigate host–microbe interactions. Our experiments demonstrate that changes in the microbiome are associated with intestinal tumor formation and highlight an important role of the epithelial barrier in maintaining host–microbe homeostasis. We provide several lines of evidence that intestinal tumorigenesis results in severe barrier defects, which, in turn, cause dysbiosis. The dysbiotic microbiome and tumor cells form a feedback loop to further fuel tumor growth. Mechanistically, we show that tumor growth alters the expression of genes involved in the control of microbiota in the intestine, including PGRP-SC2 and Duox. Furthermore, tumorigenesis causes loss of septate junction proteins, which were previously shown to be required for strengthening the epithelium structure and to form a barrier to solute diffusion through the intercellular space (46). In addition, tumor growth alters gut morphology and give rise to a shrunken tissue. Finally, a growing tumor tissue leads to epithelium breakdown and increased intestinal permeability (Fig. 7*H*).

Functional and structural disruptions of the intestinal barrier trigger alterations in both bacterial load and composition and thereby induce commensal dysbiosis. We show that intestinal barrier failure is associated with an increase in JNK activity. Our data further support a model whereby tumor-related JNK activation is responsible for intestinal barrier dysfunction, leading to commensal dysbiosis as well as immune activation and a subsequently shorter lifespan. Inhibition of tumor growth or JNK inhibition reverses these phenotypes. Moreover, microbial elimination restores intestinal barrier function and delays tumor growth, which can extend the lifespan of tumor-bearing animals.

Self-Enforcement between Tumor and the Dysbiotic Microbiome. In *Drosophila*, intestinal commensals have been recognized as important factors that influence gut immunity and homeostasis (47, 48). For example, microbiota-mediated ERK signaling in ECs is required for an epithelial response to restrict intestinal viral infections (26). Our data show that tumor growth causes the reduction of microbial diversity. Previous studies indicated that reduced microbial diversity may increase the risk of susceptibility to infection and stress. In humans, a significantly lower microbiota diversity has been reported in colorectal cancer (49, 50). Furthermore, several bacterial species such as *Streptococcus bovis*, *Helicobacter pylori*, *Bacteroides fragilis*, *Enterococcus faecalis*, *Clostridium septicum*, *Fusobacterium* spp., and *Escherichia coli* have been associated with colorectal carcinogenesis (51), although the causal link remains unclear. Our data also demonstrate that microbial clearance reduces proliferative and inflammatory signals in tumor intestine with a decreased stem cell activity, indicating the dysbiotic microbiome create a proinflammatory environment that promotes tumor growth. Consistent with this, studies in insect models suggested that microbial dysbiosis by dysregulating the immune regulator Nub-PB, or oral infection with commensals promotes proinflammatory signatures and the activation of JAK/STAT and JNK signaling in the intestine (52, 53). It has also been shown that aging-related intestinal dysbiosis occurs before intestinal barrier dysfunction (36, 37). In aged flies, intestinal barrier dysfunction is associated with intestinal and systemic inflammation (36, 40). In aged intestine, changes in microbiome follow intestinal barrier dysfunction, leading to systemic inflammation and animal death (36). However, whether the tumor-related changes in microbiota occur before or after intestinal barrier dysfunction remains unclear and needs further investigations.

Tumor Growth Causes Intestinal Dysfunction and Dysbiosis. In response to infection, the intestinal epithelium undergoes severe morphological changes, while retaining the ability to recover within a few hours (54). Barrier dysfunction has been correlated with impaired insulin and immune signaling (40). Our experiments show that tumor growth impairs barrier function by inducing gut integrity loss, immune activation, reduced *Duox* expression, and in turn causes intestinal dysbiosis. This is consistent with previous results showing that intestinal barrier failure after loss of a septate junction protein Snakeskin (Ssk) results in altered gut morphology, dysbiosis, and reduced *Duox* level (37). *Duox* act as an important defense mechanism in ECs against enteric infection and its expression is increased in the intestine upon infection and aging (20, 55), while its expression is dampened in the tumor-bearing intestine with massive loss of ECs and impaired EC renewal capacity. A recent study demonstrated lactic acid from *L. plantarum* activates *Nox* for ROS production that promotes intestinal damage and dysplasia (21). Increased ROS levels are also detected in the vicinity of *Sox21a* tumors (6). However, molecular evidence on how ROS levels are regulated during tumorigenesis is still lacking and further studies are needed to investigate whether an increased microbiota also trigger intestinal ROS level through *Nox* for tumor progression. Previous studies demonstrate that BMP signaling is required for CCR function and aging-related decline in CCR has been linked to microbial dysbiosis (22, 29). Our results indicate that tumor related intestinal dysbiosis is independent of CCR decline. The gastric stem cells in the CCR are largely quiescent and only can be induced to regenerate the gastric epithelium upon challenge (56). We therefore speculate that the CCR decline related to microbiota changes occurs only at regenerative or aging conditions, whereas the tumor growth does not alter the CCR identity at a young age. Notably, tumor growth also leads to a decrease in gut length. Patel et al. (3) demonstrated that tumor cells compete with nearby ECs and induce EC detachment and cell death. They also reported that a mutation in Notch inhibits differentiation in the stem cell lineage and leads to impaired EC renewal and tumor formation. We previously showed that loss of BMP signaling leads to blockage in EC differentiation and growth (32). Therefore, similar mechanism may occur in tumors caused by loss of BMP signaling, where EC apoptosis and impaired EC renewal could lead to a decrease in gut length.

JNK Activation Contributes to Tumorigenesis and Epithelial Barrier Failure. In this study, we showed that *Mmp1* and *Mmp2* expression is associated with tumor progression and reducing Mmp2 expression dampens the tumor growth. In line with this result, the expression of JNK downstream effectors Mmp1 and Mmp2 has been described to be induced in EBs of *Sox21a* tumor (6). EB-specific Mmp2 depletion in *Sox21a* flies reduced tumor burden and growth toward the lumen (6). The matrix metalloproteinases (MMPs) are involved in extracellular matrix (ECM) component cleavage (57). Therefore, the JNK-mediated MMP expression may be involved in ECM degradation and facilitates tumor growth or induces cell death to adjacent ECs. Consequently, tumor growth requires JNK-related MMP expression. Tumor cell migration has been reported in *Drosophila* larval eye/antenal imaginal disc or hindgut. For example, Uhlirova et al. (58) reported that JNK/Mmp1 activity is required for the migration of rasV12, scrib− tumor cells in the larval eye/antennal imaginal disc. In addition, the activation of JNK/Mmp1 signaling triggers rasV12 related cell migration in *Drosophila* hindgut. Ingestion of commensals, such as *Pseudomonas aeruginosa*, enhances rasV12-mediated cell migration, suggesting that the microbiota influences tumor-related phenotypes (59). However, there is to date no evidence that BMP signaling inactivation induces tumor cell migration in the presence or absence of JNK activation.

In mammals, JNK activity affects cell proliferation, differentiation, survival, and migration in a context-dependent manner and these events have also been linked to tumorigenesis (60). Our data also indicate the increased JNK activity causes intestinal barrier failure. Dampening JNK signaling might be an effective strategy to prevent loss of barrier function, microbial dysbiosis, and tumor progression. Recent studies identified a combinatorial strategy to limit tumor growth in a *Drosophila* hindgut model by targeting the PI3K pathway (61). This was further supported by similar effects in mouse models of colorectal cancer (61), indicating that key pathways might play evolutionarily conserved roles during tumorigenesis. Based on data presented, it would be interesting to further investigate the JNK inhibitory effect in mammalian intestinal cancer models.

Conclusions

Our study uncovers an important role of JNK signaling in controlling epithelial barrier function in order to maintain host–microbe homeostasis. Intestinal tumors activate JNK signaling, which enhances tumor growth and barrier dysfunction. The impaired intestinal barrier disrupts host–microbe homeostasis and leads to dysbiosis, which initiate a proliferative or inflammatory response to further promote tumorigenesis. Interestingly, we found that JNK inhibition and microbiota depletion restores epithelial barrier function and reduces tumorigenesis. Therefore, combinatorial targeting of a tumor-induced microbial dysbiosis and stress signaling pathways in tumor cells could delay tumor growth and prevent intestinal dysfunction.

Materials and Methods

***Drosophila* Culture and Medium.** Animals were reared at either 18 °C or 29 °C with a 12-h light cycle with 60% humidity. One liter of standard fly medium contains: 44 g sugar syrup, 80 g malt, 80 g corn flour premium G750, 10 g soy flour, 18 g yeast, 2.4 g methly-4-hydroxybenzoate, 6.6 mL propionicacid, 0.66 mL phosphoricacid, and 8 g agar, as also previously described (62). Antibiotic treatment was conducted by adding 150 μg/mL carbenicillin, 150 μg/mL metronidazole, and 75 μg/mL tetracyclin to standard fly food. The antibiotic mixture was added to the food at a suitable temperature to prevent heat inactivation. Animals in control or experimental groups were transferred to fresh food every 2 d to prevent fungal infection.

Fly Stocks. esg^{ts}F/O (33) (esg-Gal4,UAS-GFP; Act > CD2 > Gal4, TubGal80), Myol^{ts}, MyoIA-lacZ (63), UAS-Hep^{ACT}, Puc^{E69} (33), UAS-Notch-RNAi (3), esg^{ts} and Dl-lacZ (kind gift of Bruce Edgar, University of Utah, Salt Lake City, UT), UAS-Upd2 (6), UAS-Upd2-RNAi (6), UAS-Mmp1 (58), UAS-Mmp2 (58), UAS-Kay-RNAi (58), UAS-Mmp2-RNAi (58) (kind gift of Mirka Uhlirova, University of Cologne, Cologne, Germany), (BLN6397), UAS-Mad-RNAi^{Trip} (BLN31315), UAS-Med-RNAi^{KK} (KK108412, VDRC), UAS-Shn-RNAi^{KK} (KK101278, VDRC), UAS-Mad-RNAi^{KK} (KK110517, VDRC), UAS-Mad-RNAi^{GD} (GD12635, VDRC), UAS-Med-RNAi^{GD-1} (GD19688, VDRC) UAS-Mad-RNAi^{GD-2} (GD19689, VDRC), UAS-Bsk^{DN} (33) (BLN6409), UAS-Cas9.P2 (64), and guide-RNA transgenic strains (this study): sepia-gRNA^{2X}, Mad-gRNA^{2X}, Med-gRNA^{2X}. Nubbin-Gal4 driven Mad-RNAi^{Trip}, Med-RNAi^{KK} and Shn-RNAi^{KK} were previously tested to cause Dpp/BMP loss-of-function phenotype with small wings and vein formation loss (32). Shn-RNAi^{KK} results in stronger wing phenotype than Med-RNAi^{KK} or Mad RNAi^{Trip} (32). The KK RNAi lines used in this study were tested negative by PCR for a tiptop off-target phenotype caused by an additional insertion at the 40D locus (65).

Axenic Condition Experiments. To generate germ-free flies, embryos were collected on grape juice plates. Briefly, embryos less than 12 h old were washed with 1× PBS and then rinsed in 70% ethanol. After that, embryos were bleached with 3% solution of sodium hypochlorite for 2 to 3 min and washed with sterile water three times. Axenic embryos were then transferred to autoclaved medium in a sterile hood and maintained at 18 °C. Subsequent generations were maintained in parallel to their conventionally reared counterparts by transferring adults to new sterile tubes in a separate sterile box at 29 °C for RNAi induction. Axenic conditions were confirmed by 16S rDNA bacterial qPCR, as described previously (20, 66).

***Drosophila* Lifespan Assay.** One bottle containing 20 virgin females (*esg^{ts}F/O, MyoIA^{ts}* drivers) and 5 to 7 males (RNAi transgenes or controls) were used to make a cross. Progenies were collected in 3 d after eclosion. Around 80 females plus 20 males with indicated genotype were transferred to a cage and incubated at 29 °C to induce RNAi effect. At least three biological replicates for each genotype were prepared for each experiment. The food was changed every 2 to 3 d to prevent fly drown into food or fungal growth. Only the dead female flies were counted during aging and the data were analyzed using PRISM 6 statistical software. The same mixture of antibiotics as described above was used to generate antibiotic containing food for the lifespan assay on bacteria-depleted environment. The lifespan assay has been performed three times and only one experiment is shown in the related figure.

Generation of Short-Guide RNA Transgenic Stocks. Transgenic short-guide RNA (sgRNA) stocks (Mad-gRNA2X-HD_CFD00651 and Med-gRNA2X-HD_CFD00386) were generated as part of the Heidelberg CRISPR fly library. Target sites were identified using E-CRISP (a web application to design gRNA sequences) (67) and pairs of sgRNAs, targeting the 5′ portion of the coding sequence, were cloned into pCFD6, using methods described previously (68). Plasmids were integrated at attP40 on the second chromosome using PhiC31-mediated integration and confirmed by Sanger sequencing. The gRNAs sequences are Mad-sgRNA1-TGTGTTCGATTCCACATCGT; Mad-sgRNA2-TGGCGAGGAACGAGTACTGG; Med-sgRNA1- GTGGGGGCGTTCGAGGGCGG; Med-sgRNA2-GTCCGGCCTGAGTCTGCAGT.

Tissue-Specific CRISPR/Cas9-Mediated Mutagenesis. The expression of Cas9 is temporally controlled by *UAS/Gal4/Gal80ts* system in the intestinal stem cell compartments (*escargot-Gal4; Tubulin-Gal80^{ts}; UAS-Cas9* and in short: *esg^{ts}, UAS-Cas9*). The Mad or Med gRNAs male flies were crossed with the driver *esg^{ts} > UAS-Cas9* at 18 °C to prevent the misexpression of Cas9 during the fly development. Their progeny with the right genotype (*esg^{ts}, UAS-Cas9 > UAS- t::gRNA-Mad^{2X}* or *UAS-t::gRNA-Med^{2X}*) were collected and shifted to 29 °C to activate Cas9 expression for 5 d. Afterward, the flies were maintained at 18 °C until being killed for the experiments. Note that *esgts*-driven Cas9 and sgRNAs is expressed only for 5 d to induce mutations and then animals are shifted to 18 °C. No GFP expression is observed as *esg-GFP* is repressed by tubGal80 at 18 °C. In general, we observed a higher phenotypic variability in CRISPR as compared to RNAi experiments which are likely caused by genetic mosaics of edited cells, as previously described (68). To determine the CRISPR on-target efficiency, genomic DNA was extracted from 20 dissected intestine of CRISPR-Cas9 edited flies (genotype: *esg^{ts}, UAS-Cas9 > Med-gRNA^{2X}*) and the genomic locus surrounding the sgRNA target sites was amplified by PCR. PCR amplicons were subjected to Sanger sequencing, and the resulting chromatographs were analyzed by inference of CRISPR edits analysis (https://ice.synthego.com).

Epithelial Barrier Assay and pH Measurements. The barrier defect assay (smurf assay) was conducted as described previously (40). Briefly, more than 60 flies were maintained on standard food until the day of the smurf assay. Blue dye food was prepared by adding 2.5% (wt/vol) bromophenol blue (Sigma) to normal food, which was also used as pH indicator to assay the acidity of copper cell region, as previously described (22). Flies were fed for 12 h and then monitored for the proportion of animals with a phenotype as an indicator for epithelial barrier dysfunction. To check for pH, intestines containing pH indicator were dissected in PBS. The head and posterior part were maintained intact to avoid the dye leakage. To avoid color change due to tissue incubation in PBS, images were taken immediately after dissection.

Midgut qRT-PCR. RNA was extracted from 10 midguts (females) using RNeasy (Qiagen). One microgram of RNA was reverse transcribed using the RevertAid H Minus First Strand cDNA Synthesis Kit (Fermentas). qRT-PCR was performed in a 384-well format using the Universal Probe Library or SyBr green qPCR master-mix on a LightCycler 480 (Roche). qPCR primer sequences used in this study are listed in *SI Appendix*, Table S2. At least three biological replicates ($n \geq 3$) and two independent experiments were performed. All results are presented as the means ± SD of the biological replicates. RP49 was used as a normalization control and the qPCR data are analyzed by ΔΔCT method as previously described (62).

JNK Inhibitor and Antibiotic Treatment. Flies were fed with 1 mg/mL JNK inhibitor SP600125 in 5% sucrose solution. For the combination of JNK inhibitor and antibiotics treatment, the same concentration of SP600125 was used plus an antibiotic mixture (150 μg/mL ampicillin, 150 μg/mL metronidazole and 75 μg/mL tetracyclin) solved in 5% sucrose solution. Flies were fed on a

round filter paper disk with SP600125, antibiotic mixture or a combined solution and transferred to a freshly prepared vial every day to prevent evaporation effects.

Intestinal Microbiota Assays by 16S rDNA qPCR and CFUs. The outside surface of animals was sterilized with 100% ethanol for 1 to 2 min, as previously described (36, 66), and washed twice with sterile PBS. The intestine was dissected in sterile PBS with sterile equipment. The intact tissue was carefully taken to prevent loss of lumen contents and malpighian tubules were carefully removed. The dissected intestines were stored at −80 °C before analysis. Genomic DNA extraction was performed as described in the manufacturer's protocol (PowerSoil DNA isolation Kit, MoBio). Fifteen flies were dissected for each sample to extract DNA. The bacterial load of *Alphaproteobacteria*, *Gammaproteobacteria*, *Bacilli*, and total bacteria, different families of bacteria (*Acetobacteraceae*) and *L. plantarum* were measured by qPCR with primers listed in *SI Appendix*, Table S1. qPCR results were normalized with *Drosophila* Actin5C as previously described (36, 43, 69). For CFU assays, animals were surface sterilized as described above and five intestines were dissected and homogenized in 500 μL PBS. Three serial dilutions of 1:10 on the homogenates were plated on selective plates for *Acetobacteraceae*, *Lactobacili*, and nutrient-rich medium (see information for the protocols in *SI Appendix, Supplementary Methods*). The plates were incubated at 29 °C and colonies were counted after 48 and 72 h, as previously described (70). At least two independent experiments were performed and each with at least four biological replicates ($n \geq 4$).

16S rDNA Sequencing. To obtain bacterial genomic DNA (gDNA) from the intestine, flies were surface-sterilized before dissection as described above. Whole midguts were maintained as intact tissues to prevent bacterial leakage and the crops of fly guts were removed. Thirty guts were dissected for each sample and the gDNA was extracted using PowerSoil DNA isolation kit (MoBio). The gDNA was used to generate amplicons that cover V3 and V4 hypervariable regions of bacteria and Archaea 16S rDNA. Indexed adapters were added to the end of the 16S rDNA amplicons by limited cycle PCR to prepare sequencing library. DNA libraries were multiplexed and sequenced on an Illumina MiSeq instrument.

Histology. Antibody staining was performed as previously described (62). TUNEL staining was performed based on the instruction of the ApopTag Red in situ detection kit (Millipore S7165). Antibodies were used at the following final concentrations: Anti-Discs large (1:1,200), anti-FasIII (1:1,000), anti–β-galactosidase (1:1,000), antiphospho JNK (1:600), anti-pH3 (1:600), anti-Cas3 (1:800), anti-DCP1 (1:600). All secondary antibodies were diluted at a final concentration of 1:3,000. The detailed information is provided in *SI Appendix*, Table S3.

Quantification and Statistical Analysis. For all quantifications, n equals the number of midguts used in the experiment. The results are presented as mean ± SEM. Comparisons between groups were made using the unpaired two-tailed Student's t test. Statistical analyses for survival curves were performed using the log-rank (Mantel-Cox) test. The significance between groups was expressed as P values: $^{*}P < 0.05$, $^{**}P < 0.01$, $^{***}P < 0.001$, and "ns" denotes no significant difference.

Quantification of pH3 Cell Counts per Midgut. Mitotic cells marked by phospho-histone 3 staining were counted in the intestine of indicated genotypes. Approximately 10 midguts were dissected and counted in each experiment and data from three independent experiments are shown. The results are presented as mean value of cell counts with SD in the bar figures. Experiments were conducted as described previously (62).

Data Availability. All data are available within this manuscript and the associated *SI Appendix*.

ACKNOWLEDGMENTS. We thank M. Funk, F. Heigwer, F. Port, and J. Bageritz for comments on the manuscript; B. Edgar, M. Uhlirova, X. Yang, the Bloomington Drosophila Stock Center, and Vienna Drosophila Resource Center for fly stocks and antibodies; F. Port for CRISPR lines; and K. Han (Institute of Pharmacy and Molecular Biology, Heidelberg University) and M.B. laboratory members for helpful discussions and experimental support, especially S. H. Wang, L. Lai, D. Tasqin, J. Mattila, J. Bageritz, B. Rauscher, and A.-L. Boettcher. We also thank the Imaging Core and Genomics and Proteomics Core Facilities at the German Cancer Research Center for support. Research in the laboratory of M.B. is supported in part by the Deutsche Forschungsgemeinschaft Collaborative Research Center SFB873 and the Excellence Cluster CellNetworks.

1. I. Miguel-Aliaga, H. Jasper, B. Lemaitre, Anatomy and physiology of the digestive tract of *Drosophila melanogaster*. *Genetics* **210**, 357–396 (2018).
2. Z. Guo, I. Driver, B. Ohlstein, Injury-induced BMP signaling negatively regulates Drosophila midgut homeostasis. *J. Cell Biol.* **201**, 945–961 (2013).
3. P. H. Patel, D. Dutta, B. A. Edgar, Niche appropriation by Drosophila intestinal stem cell tumours. *Nat. Cell Biol.* **17**, 1182–1192 (2015).
4. A. Ragab *et al*., Drosophila Ras/MAPK signalling regulates innate immune responses in immune and intestinal stem cells. *EMBO J.* **30**, 1123–1136 (2011).
5. S. J. E. Suijkerbuijk, G. Kolahgar, I. Kucinski, E. Piddini, Cell competition drives the growth of intestinal adenomas in Drosophila. *Curr. Biol.* **26**, 428–438 (2016).
6. Z. Zhai *et al*., Accumulation of differentiating intestinal stem cell progenies drives tumorigenesis. *Nat. Commun.* **6**, 10219 (2015).
7. J. B. Cordero, R. K. Stefanatos, K. Myant, M. Vidal, O. J. Sansom, Non-autonomous crosstalk between the Jak/Stat and Egfr pathways mediates Apc1-driven intestinal stem cell hyperplasia in the Drosophila adult midgut. *Development* **139**, 4524–4535 (2012).
8. J.-P. Parvy, J. A. Hodgson, J. B. Cordero, *Drosophila* as a model system to study non-autonomous mechanisms affecting tumour growth and cell death. *BioMed Res. Int.* **2018**, 7152962 (2018).
9. K. Siudeja *et al*., Frequent somatic mutation in adult intestinal stem cells drives neoplasia and genetic mosaicism during aging. *Cell Stem Cell* **17**, 663–674 (2015).
10. N. Buchon, N. A. Broderick, B. Lemaitre, Gut homeostasis in a microbial world: Insights from Drosophila melanogaster. *Nat. Rev. Microbiol.* **11**, 615–626 (2013).
11. J. L. Round, S. K. Mazmanian, The gut microbiota shapes intestinal immune responses during health and disease. *Nat. Rev. Immunol.* **9**, 313–323 (2009).
12. L. V. Hooper, D. R. Littman, A. J. Macpherson, Interactions between the microbiota and the immune system. *Science* **336**, 1268–1273 (2012).
13. H. Tilg, T. E. Adolph, R. R. Gerner, A. R. Moschen, The intestinal microbiota in colorectal cancer. *Cancer Cell* **33**, 954–964 (2018).
14. G. Storelli *et al*., Lactobacillus plantarum promotes Drosophila systemic growth by modulating hormonal signals through TOR-dependent nutrient sensing. *Cell Metab.* **14**, 403–414 (2011).
15. R. Yamada, S. A. Deshpande, K. D. Bruce, E. M. Mak, W. W. Ja, Microbes promote amino acid harvest to rescue undernutrition in Drosophila. *Cell Rep.* **10**, 865–872 (2015).
16. D. R. Sannino, A. J. Dobson, K. Edwards, E. R. Angert, N. Buchon, The *Drosophila melanogaster* gut microbiota provisions thiamine to its host. *MBio* **9**, e00155-18 (2018).
17. M. E. Martino *et al*., Bacterial adaptation to the host's diet is a key evolutionary force shaping Drosophila-Lactobacillus symbiosis. *Cell Host Microbe* **24**, 109–119.e6 (2018).
18. A. R. Reedy, L. Luo, A. S. Neish, R. M. Jones, Commensal microbiota-induced redox signaling activates proliferative signals in the intestinal stem cell microenvironment. *Development* **146**, dev171520 (2019).
19. L. Kamareddine, W. P. Robins, C. D. Berkey, J. J. Mekalanos, P. I. Watnick, The Drosophila immune deficiency pathway modulates enteroendocrine function and host metabolism. *Cell Metab.* **28**, 449–462.e5 (2018).
20. L. Guo, J. Karpac, S. L. Tran, H. Jasper, PGRP-SC2 promotes gut immune homeostasis to limit commensal dysbiosis and extend lifespan. *Cell* **156**, 109–122 (2014).
21. I. Iatsenko, J.-P. Boquete, B. Lemaitre, Microbiota-derived lactate activates production of reactive oxygen species by the intestinal NADPH oxidase Nox and shortens Drosophila lifespan. *Immunity* **49**, 929–942.e5 (2018).
22. H. Li, Y. Qi, H. Jasper, Preventing age-related decline of gut compartmentalization limits microbiota dysbiosis and extends lifespan. *Cell Host Microbe* **19**, 240–253 (2016).
23. F. Obata *et al*., Nutritional control of stem cell division through S-adenosylmethionine in Drosophila intestine. *Dev. Cell* **44**, 741–751.e3 (2018).
24. B. Erkosar *et al*., Pathogen virulence impedes mutualist-mediated enhancement of host juvenile growth via inhibition of protein digestion. *Cell Host Microbe* **18**, 445–455 (2015).
25. R. M. Jones *et al*., Lactobacilli modulate epithelial cytoprotection through the Nrf2 pathway. *Cell Rep.* **12**, 1217–1225 (2015).
26. C. L. Sansone *et al*., Microbiota-dependent priming of antiviral intestinal immunity in Drosophila. *Cell Host Microbe* **18**, 571–581 (2015).
27. B. Charroux *et al*., Cytosolic and secreted peptidoglycan-degrading enzymes in Drosophila respectively control local and systemic immune responses to microbiota. *Cell Host Microbe* **23**, 215–228.e4 (2018).
28. C. N. Fischer *et al*., Metabolite exchange between microbiome members produces compounds that influence *Drosophila* behavior. *eLife* **6**, e18855 (2017).
29. H. Li, Y. Qi, H. Jasper, Dpp signaling determines regional stem cell identity in the regenerating adult Drosophila gastrointestinal tract. *Cell Rep.* **4**, 10–18 (2013).
30. A. Tian, J. Jiang, Intestinal epithelium-derived BMP controls stem cell self-renewal in Drosophila adult midgut. *eLife* **3**, e01857 (2014).
31. A. Tian, B. Wang, J. Jiang, Injury-stimulated and self-restrained BMP signaling dynamically regulates stem cell pool size during *Drosophila* midgut regeneration. *Proc. Natl. Acad. Sci. U.S.A.* **114**, E2699–E2708 (2017).
32. J. Zhou *et al*., Dpp/Gbb signaling is required for normal intestinal regeneration during infection. *Dev. Biol.* **399**, 189–203 (2015).
33. H. Jiang *et al*., Cytokine/Jak/Stat signaling mediates regeneration and homeostasis in the Drosophila midgut. *Cell* **137**, 1343–1355 (2009).
34. D. Vandeputte *et al*., Quantitative microbiome profiling links gut community variation to microbial load. *Nature* **551**, 507–511 (2017).

35. J.-H. Ryu *et al*., Innate immune homeostasis by the homeobox gene caudal and commensal-gut mutualism in Drosophila. *Science* **319**, 777–782 (2008).
36. R. I. Clark *et al*., Distinct shifts in microbiota composition during Drosophila aging impair intestinal function and drive mortality. *Cell Rep.* **12**, 1656–1667 (2015).
37. A. M. Salazar *et al*., Intestinal Snakeskin limits microbial dysbiosis during aging and promotes longevity. *iScience* **9**, 229–243 (2018).
38. D. M. Bryant, K. E. Mostov, From cells to organs: Building polarized tissue. *Nat. Rev. Mol. Cell Biol.* **9**, 887–901 (2008).
39. E.-S. Oh, M. Seiki, M. Gotte, J. Chung, Cell adhesion in cancer. *Int. J. Cell Biol.* **2012**, 965618 (2012).
40. M. Rera, R. I. Clark, D. W. Walker, Intestinal barrier dysfunction links metabolic and inflammatory markers of aging to death in Drosophila. *Proc. Natl. Acad. Sci. U.S.A.* **109**, 21528–21533 (2012).
41. K.-A. Lee *et al*., Bacterial uracil modulates Drosophila DUOX-dependent gut immunity via Hedgehog-induced signaling endosomes. *Cell Host Microbe* **17**, 191–204 (2015).
42. E. Martín-Blanco *et al*., Puckered encodes a phosphatase that mediates a feedback loop regulating JNK activity during dorsal closure in Drosophila. *Genes Dev.* **12**, 557–570 (1998).
43. J. Sebald *et al*., Impact of the chromatin remodeling factor CHD1 on Gut microbiome composition of Drosophila melanogaster. *PLoS One* **11**, e0153476 (2016).
44. Y. Kwon *et al*., Systemic organ wasting induced by localized expression of the secreted insulin/IGF antagonist ImpL2. *Dev. Cell* **33**, 36–46 (2015).
45. J. C. Hardwick, L. L. Kodach, G. J. Offerhaus, G. R. van den Brink, Bone morphogenetic protein signalling in colorectal cancer. *Nat. Rev. Cancer* **8**, 806–812 (2008).
46. A. Hijazi *et al*., Boudin is required for septate junction organisation in Drosophila and codes for a diffusible protein of the Ly6 superfamily. *Development* **136**, 2199–2209 (2009).
47. N. Buchon *et al*., Morphological and molecular characterization of adult midgut compartmentalization in Drosophila. *Cell Rep.* **3**, 1725–1738 (2013).
48. W.-J. Lee, P. T. Brey, How microbiomes influence metazoan development: Insights from history and Drosophila modeling of gut-microbe interactions. *Annu. Rev. Cell Dev. Biol.* **29**, 571–592 (2013).
49. N. Wu *et al*., Dysbiosis signature of fecal microbiota in colorectal cancer patients. *Microb. Ecol.* **66**, 462–470 (2013).
50. W. Chen, F. Liu, Z. Ling, X. Tong, C. Xiang, Human intestinal lumen and mucosa-associated microbiota in patients with colorectal cancer. *PLoS One* **7**, e39743 (2012).
51. J. Gagnière *et al*., Gut microbiota imbalance and colorectal cancer. *World J. Gastroenterol.* **22**, 501–518 (2016).
52. B. G. Lindberg *et al*., Nubbin isoform antagonism governs *Drosophila* intestinal immune homeostasis. *PLoS Pathog.* **14**, e1006936 (2018).
53. J. Lin *et al*., Gene expression profiling provides insights into the immune mechanism of *Plutella xylostella* midgut to microbial infection. *Gene* **647**, 21–30 (2018).
54. K.-Z. Lee *et al*., Enterocyte purge and rapid recovery is a resilience reaction of the gut epithelium to pore-forming toxin attack. *Cell Host Microbe* **20**, 716–730 (2016).
55. K.-A. Lee *et al*., Inflammation-modulated metabolic reprogramming is required for DUOX-dependent gut immunity in Drosophila. *Cell Host Microbe* **23**, 338–352.e5 (2018).
56. M. Strand, C. A. Micchelli, Quiescent gastric stem cells maintain the adult Drosophila stomach. *Proc. Natl. Acad. Sci. U.S.A.* **108**, 17696–17701 (2011).
57. K. Kessenbrock, V. Plaks, Z. Werb, Matrix metalloproteinases: Regulators of the tumor microenvironment. *Cell* **141**, 52–67 (2010).
58. M. Uhlirova, D. Bohmann, JNK- and Fos-regulated Mmp1 expression cooperates with Ras to induce invasive tumors in *Drosophila*. *EMBO J.* **25**, 5294–5304 (2006).
59. E. Bangi, C. Pitsouli, L. G. Rahme, R. Cagan, Y. Apidianakis, Immune response to bacteria induces dissemination of Ras-activated *Drosophila* hindgut cells. *EMBO Rep.* **13**, 569–576 (2012).
60. C. Bubici, S. Papa, JNK signalling in cancer: In need of new, smarter therapeutic targets. *Br. J. Pharmacol.* **171**, 24–37 (2014).
61. E. Bangi, C. Murgia, A. G. Teague, O. J. Sansom, R. L. Cagan, Functional exploration of colorectal cancer genomes using *Drosophila*. *Nat. Commun.* **7**, 13615 (2016).
62. J. Zhou, B. A. Edgar, M. Boutros, ATF3 acts as a rheostat to control JNK signalling during intestinal regeneration. *Nat. Commun.* **8**, 14289 (2017).
63. H. Jiang, M. O. Grenley, M.-J. Bravo, R. Z. Blumhagen, B. A. Edgar, EGFR/Ras/MAPK signaling mediates adult midgut epithelial homeostasis and regeneration in Drosophila. *Cell Stem Cell* **8**, 84–95 (2011).
64. F. Port, H.-M. Chen, T. Lee, S. L. Bullock, Optimized CRISPR/Cas tools for efficient germline and somatic genome engineering in Drosophila. *Proc. Natl. Acad. Sci. U.S.A.* **111**, E2967–E2976 (2014).
65. J. H. A. Vissers, S. A. Manning, A. Kulkarni, K. F. Harvey, A Drosophila RNAi library modulates Hippo pathway-dependent tissue growth. *Nat. Commun.* **7**, 10368 (2016).
66. N. Buchon, N. A. Broderick, S. Chakrabarti, B. Lemaitre, Invasive and indigenous microbiota impact intestinal stem cell activity through multiple pathways in Drosophila. *Genes Dev.* **23**, 2333–2344 (2009).
67. F. Heigwer, G. Kerr, M. Boutros, E-CRISP: Fast CRISPR target site identification. *Nat. Methods* **11**, 122–123 (2014).
68. F. Port, S. L. Bullock, Augmenting CRISPR applications in Drosophila with tRNA-flanked sgRNAs. *Nat. Methods* **13**, 852–854 (2016).
69. M. J. Claesson *et al*., Comparison of two next-generation sequencing technologies for resolving highly complex microbiota composition using tandem variable 16S rRNA gene regions. *Nucleic Acids Res.* **38**, e200 (2010).
70. N. A. Broderick, N. Buchon, B. Lemaitre, Microbiota-induced changes in drosophila melanogaster host gene expression and gut morphology. *MBio* **5**, e01117-14 (2014).